



Advection-Dominated Transport Dynamics of Pili and Flagella-Mediated Motile Bacteria in Porous Media

Journal:	<i>Soft Matter</i>
Manuscript ID	SM-ART-01-2025-000071.R1
Article Type:	Paper
Date Submitted by the Author:	13-Mar-2025
Complete List of Authors:	Berghouse, Marc; Desert Research Institute; University of Nevada Reno, GPHS Perez, Lazaro; Oregon State University, Department of Civil and Construction Engineering Plymale, Andrew; Pacific Northwest National Laboratory Scheibe, Timothy; Pacific Northwest National Laboratory Parashar, Rishi; Desert Research Institute,

Advection-Dominated Transport Dynamics of Pili and Flagella-Mediated Motile Bacteria in Porous Media

Marc Berghouse^{†,‡}, Lazaro J. Perez^{||}, Andrew Plymale⁺, Timothy D. Scheibe⁺⁺, & Rishi Parashar^{†,*}

[†] *Division of Hydrologic Science, Desert Research Institute, Reno, Nevada, 89512*

[‡] *Graduate Program of Hydrologic Sciences, University of Nevada, Reno, Reno, Nevada, 89557*

^{||} *Department of Civil and Construction Engineering, Oregon State University, Corvallis, Oregon, 97331*

⁺ *Energy and Environment Directorate, Pacific Northwest National Laboratory, Richland, Washington, 99354*

⁺⁺ *Earth and Biological Sciences Directorate, Pacific Northwest National Laboratory, Richland, Washington, 99354*

Corresponding Author: Rishi Parashar

Email: Marc.Berghouse@dri.edu, lazaro.perez@oregonstate.edu, plymale@pnnl.gov, tim.scheibe@pnnl.gov, Rishi.Parashar@dri.edu*

Phone Number of Corresponding Author: +1 775 673 7496

Author Contributions: R.P. and T.D.S. designed research. L.J.P performed experiments. A.P. cultured bacteria and advised on biological aspects of the experiments. M.B. conducted simulations of microfluidic models and analyzed experimental data. M.B., L.J.P., and R. P. interpreted the modeling results. M.B., L.J.P., R.P., and A.P. wrote the paper.

Competing Interest Statement: The authors declare no competing interests.

Preprint Server: N/A

Keywords: Bacterial Transport, Motility, Porous Media

1 **Abstract**

2 The transport of motile bacteria in porous media is highly relevant to many fields, ranging from ecology to
3 human health. Still, critical gaps remain in our understanding of the impacts of hydrodynamics and pore
4 structure on bacterial transport. Here, we present direct visualizations of three species of motile bacteria
5 under variable flow rates and porosities. We find that at higher flow rates, motility is less critical to the
6 transport of bacteria, as motion is controlled by hydrodynamic advection, making it difficult for bacteria to
7 move across streamlines. We show that this lack of motion across streamlines results in increased velocity
8 autocorrelation and bacterial spreading in the direction of flow. Furthermore, we find that transport of
9 bacteria with different motility types are impacted by flow rates to different extents. At low flow rates, the
10 transport of bacteria with pili-mediated twitching motility is strongly controlled by advection, whereas
11 bacteria with flagella still display active motility. At higher flow rates, we show that bacteria with
12 peritrichous flagella maintain their motility characteristics to a greater degree than bacteria with pili or
13 monotrichous flagella. We also examine experimental net speeds of bacteria in relation to the simulated
14 flow fields and find that the interactions between hydrodynamics, motility, and porous media geometry lead
15 to oversampling of medium-velocity regions of a pore network by all three species. The study presents new
16 perspectives on how different types of motile bacteria are transported and dispersed in porous media aided
17 by strength of differentially advecting fluid.

18

19 **1. Introduction**

20 Motile bacteria often live in dynamic flow environments, and their migration involves complex self-
21 propulsion strategies that are relevant to human health and ecology.¹⁻³ Navigating confined spaces of a pore
22 network, motile bacteria employ diverse movement modalities (e.g., turn angles, run-and-tumble, or run-
23 and-flick) that characterize their migration.⁴⁻⁹ In porous media, the degree of confinement (i.e., porosity)
24 and speed of the fluid flow strongly affect bacterial migration and modulate their interactions with the
25 surrounding environment. This, in turn, has a broad range of effects on bacteria, such as altering their
26 movement,¹⁰ behavior,¹¹ resource acquisition,¹² and signaling,¹³ thereby influencing their metabolic
27 functions, spatial distribution, and diversity. Spatial variations in flow velocities and the related changes in
28 shear add another level of complexity to the transport of bacteria. Transverse movement of bacteria from
29 low-shear to high-shear regions located near surfaces has been shown to result in the accumulation of cells
30 in low-velocity regions.^{14, 15} This phenomenon, termed shear trapping, has been identified as one major
31 mechanism that drives initial colonization of curved surfaces and microfluidic pore channels,¹⁶⁻¹⁸ leading
32 to the formation of suspended biofilm structures.^{19, 20} While these observations have led to improvements
33 in our understanding of bacterial transport in idealized systems, there are significant gaps in our ability to
34 quantify and predict transport behavior under complex conditions, such as in pore networks designed to
35 produce the hydrodynamics of natural porous media. Understanding the motile behavior of bacteria in
36 confined environments, in which they search for available physical space and move in response to fluid
37 flow, has implications for a wide range of applications, such as bioremediation,²¹ biofilm formation,^{22, 23}
38 and anticancer drug delivery.²⁴

39 Here, we report direct bacterial transport visualizations, at single-cell resolution, of three different species
40 of motile bacteria under variable flow conditions in a quasi-2D porous media with different levels of pore

41 confinement. Recent research conducted in microfluidic porous chips has shown that while transport of
42 non-motile bacteria is compact giving rise to a Gaussian distribution of traveled distances (i.e., follows
43 streamlines with negligible retardation due to mass exchanges between fast and slow moving zones), the
44 distribution of motile strains in the pore spaces show both active retention and enhanced dispersion due to
45 exchanges between fast flow channels and low velocity regions closer to the grain surfaces.^{17, 25} The
46 presented work here examines the transport dynamics of three motile species with an overarching goal of
47 highlighting key statistical differences in various transport metrics so that more informed modeling
48 approaches can be developed for upscaled transport simulations. Having an improved understanding of
49 dispersion rates and of the key factors that control dispersion, such as the velocity and turn angle
50 distributions, would provide robust ingredients for development of random walk based approaches.²⁵ We
51 focus on investigating transport behavior of three rod-shaped bacteria – *Acidovorax* strain JHL-9,²⁶
52 *Geobacter sulfurreducens*,²⁷ and *Paenibacillus* strain 300A²⁸ – due to their common attribute of metal-
53 reducing capabilities. By studying these specific microorganisms, our research findings are especially
54 relevant to bioremediation and biogeochemical cycling in terrestrial environments.²⁹⁻³¹ The three bacteria
55 show slight variations in size (likely overestimates due to imaging limitations) – *Acidovorax* has an average
56 body length of $10.1 \pm 2.2 \mu\text{m}$, *Geobacter* is about $8.2 \pm 1.0 \mu\text{m}$, and *Paenibacillus* is the largest at
57 $14.5 \pm 7.3 \mu\text{m}$. *Paenibacillus* have a higher ratio of body length to width than the other bacteria, although
58 direct measurement of the widths was not feasible with our experimental setup. Given that the bacteria are
59 obscured due to diffraction and long exposure times, the lengths reported here can be considered as an
60 upper bound for body size. In addition to environmental relevance, our selection of these species is based
61 on their distinct modes of motility. Using their pili to attach to surfaces and pull themselves towards new
62 locations,³² *Geobacter sulfurreducens* exhibit twitching motility.³³ *Paenibacillus* 300A exhibit swimming
63 motility, presumably driven by peritrichous flagella.³⁴ *Acidovorax* JLH-9²⁶ exhibit twitching motility,
64 consistent with genomic analysis of the strain, though transmission electron microscopy (TEM) images of
65 the strain suggest the presence of polar/monotrichous flagella, indicating the possibility of swimming
66 motility as well. Swimmers generally move much faster than twitchers,^{32, 35-37} providing a reasonable basis
67 in this study to compare the two different motility types at different flow rates. The primary focus of this
68 paper is not to decipher the fundamental reasons for differences in the transport behaviors of the three
69 selected species, but rather to evaluate transport characteristics of bioremediation relevant species with
70 different motility types in order to help lay a framework for species-aware upscaling and macroscale
71 transport simulations.

72 We find that regardless of the motility type, as flow rates increase, individual cells have trouble in moving
73 across streamlines, resulting in weaker coupling between bacterial motility and their overall transport
74 characteristics. We show that as flow speed increases, bacteria disperse faster in the direction of flow, due
75 to a lower likelihood of motion across streamlines and an increase in longitudinal displacement driven by
76 differentially advecting fluid in a porous environment. In other words, the distance between individual cells
77 grows at a fast rate since cells are less likely to make transverse movements (i.e., displacements across
78 streamlines), and are more likely to move longitudinally at a range of velocities produced by the parabolic
79 nature of laminar flow profiles. Furthermore, we show that the motility of *Paenibacillus* is less impacted
80 by flows in porous media than the motilities of *Geobacter* and *Acidovorax*, highlighting the strength of
81 peritrichous flagella-driven motility. Additionally, we provide evidence that motile bacteria tend to
82 oversample medium-velocity zones in porous media for the flow conditions tested in our experiments. This

83 work thus provides an improved picture of the transport of motile bacteria in confined porous media under
 84 variable flow rates, especially in relation to the impact of flow on different motility types, with implications
 85 for several applications where an understanding of pore-scale transport and upscaling of bacterial transport
 86 is desired.

87 2. Materials and Methods

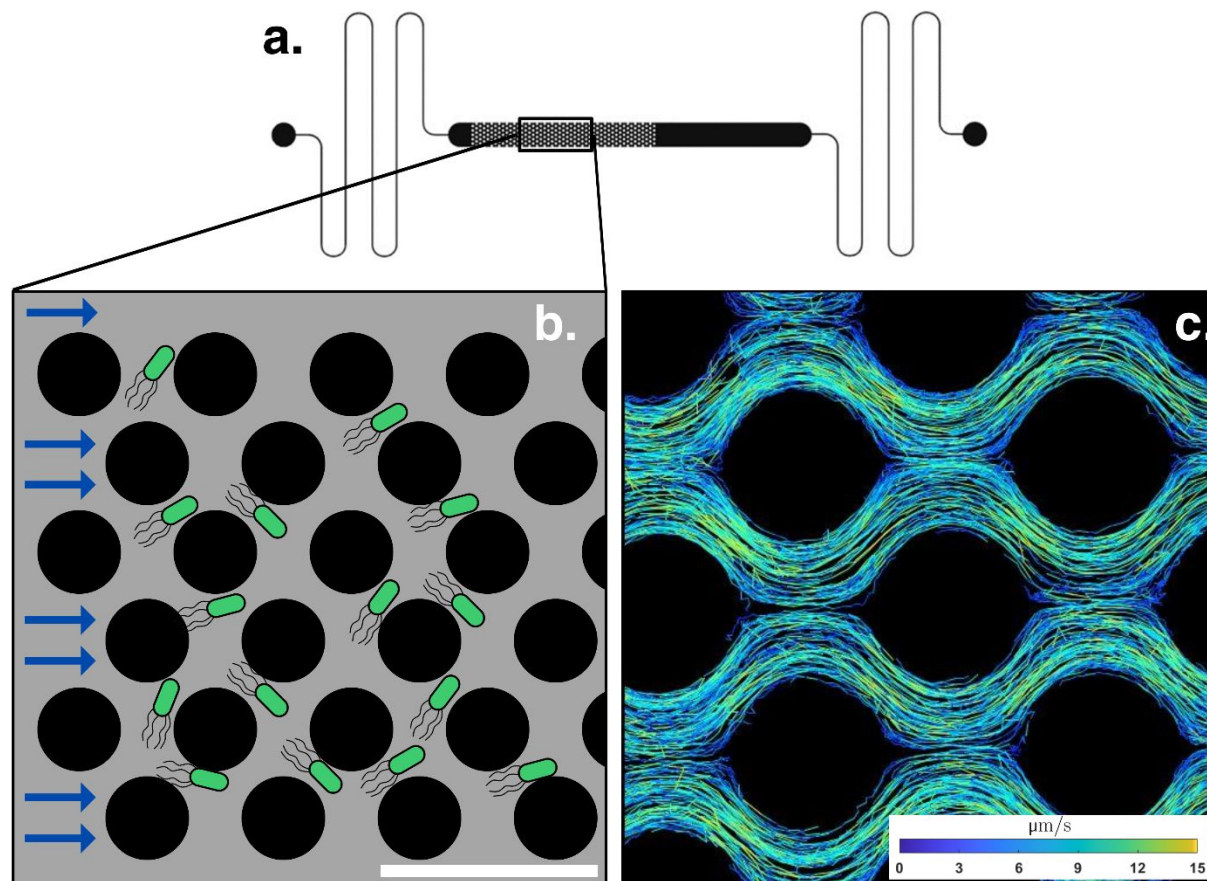
88 2.1 Bacterial Transport in Microfluidic Devices

89 To investigate the impacts of porosity, flow rate, and motility on bacterial transport, we recorded high-
 90 resolution videos of three species of bacteria swimming in microfluidic devices [2,000 μm width \times 20 μm
 91 height ($w \times h$)] at flow rates of 0 $\mu\text{L/h}$ (no flow), 1 $\mu\text{L/h}$ and 5 $\mu\text{L/h}$. The chosen flow rates allow for
 92 comparative analyses of bacterial transport for the control condition of no-flow, and when the magnitude
 93 of flow speeds and bacterial motility speeds are of a similar order. The micromodels were made from
 94 polydimethylsiloxane (PDMS) and contained staggered pillar arrays of different grain diameters and pore
 95 lengths, resulting in either low porosity ($\phi = 0.42$) or high porosity ($\phi = 0.60$) micromodels. The mean
 96 fluid speeds (v_m) determined from flow rate (Q), cross-sectional area (A), and porosity (ϕ) as $v_m = Q/A\phi$,
 97 in the low porosity geometries were 16.5 $\mu\text{m/s}$ and 82.7 $\mu\text{m/s}$, and the mean fluid speeds in the high porosity
 98 geometries were 11.6 $\mu\text{m/s}$ and 57.9 $\mu\text{m/s}$, for the low and high flow rates, respectively. These correspond
 99 to fluid speeds in the range of 1 m/day to 7.15 m/day which are medium to high-speed values typically
 100 observed in bioremediation applications in alluvial aquifer settings.^{38, 39} Assuming a characteristic length
 101 scale based on the size of the pore lengths in our porous geometries, we find that Reynolds numbers in our
 102 experiments were of the order of $\sim 10^{-3}$. We found conducting experiments at lower flow rates ($< 1 \mu\text{L/h}$)
 103 in our micromodels challenging due to pump limitations in establishing extremely low uniform rates and
 104 difficulties encountered by emergence of small drift speeds even in absence of external flow gradients
 105 presumably due to imperfections in model fabrication, small pressure aberrations at the inlet/outlet ports,
 106 small axial tilts, or potential presence of extracellular polymeric substance gradient.⁴⁰ Using pore throat
 107 length (given in section 2.2) as the characteristic length, and using the values of dispersion coefficients
 108 presented later in section 3.1.2, the velocities generated in the experiments would result in Peclet numbers
 109 approximately in the range of 0.25 to 16 – a range that allow us to make broad observations though they
 110 may be not fully generalizable. Experiments at no-flow condition in an open environment (i.e., without
 111 granular obstacles) were conducted with a subgroup of species in a previous work,⁴¹ which provides insights
 112 into the species-aware departure from Fickian diffusion in unconfined environments. After recording the
 113 videos from several replicates of experiments, we used TrackMate⁴² to track, extract, and reconstruct
 114 thousands of trajectories (ranging in length from low tens of microns to several hundred microns) of
 115 individual cells (Fig. 1).

116 To account for the small drift observed in no-flow experiments from one end of the micromodel to the
 117 other, we calculated the background flow (drift speed) by computing the rate of change in the location of
 118 the centroid as $v_d = \frac{1}{k} \sum_0^k \frac{d}{dt} (r_{cm})$, where r_{cm} is the center of mass (x and y positions) of all bacteria in a
 119 frame at no-flow, and k is the number of frames (in our case, $k = 30$). To include the greatest number of
 120 possible trajectories for this calculation, we reset the starting point of all trajectories to $t = 0$. We calculated
 121 mean drift speeds for *Acidovorax* (0.29 $\mu\text{m/s}$), *Geobacter* (1.41 $\mu\text{m/s}$) and *Paenibacillus* (0.59 $\mu\text{m/s}$)
 122 separately. These drift speeds are significantly small compared to the speeds produced in the low-flow and

123 high-flow experiments thus allowing us to treat the transport of bacteria in the two flow experiments as
 124 being solely driven by the interplay between motility and hydrodynamics.

125



126

127 **Figure 1.** Experimental setup used to analyze bacterial transport in microfluidic devices. **(a)** A sketch of the full
 128 micromodel from a previous study⁴¹ that used the same basic micromodel schematic as our experiments. The left black
 129 dot represents the inlet and the right dot represents the outlet. The black section represents an unobstructed part of the
 130 micromodel, and the gray section represents the part of the micromodel with cylinders. **(b)** Depiction of bacteria
 131 flowing (from left to right) through a section of the high porosity ($\phi = 0.60$) micromodel. The gray space represents
 132 the channels that fluid and bacteria travel through, and the black circles represent the cylinders (also referred to as
 133 “grains”). The scale bar represents $120 \mu\text{m}$. Bacteria are not drawn to scale. **(c)** Bacterial trajectories for *Acidovorax*
 134 obtained in 5-minute interval over the course of the experiment in the high porosity micromodel at a flow rate of 1
 135 $\mu\text{L/h}$. The colormap represents net speed of bacteria, with warm colors representing high speeds and cool colors
 136 representing low speeds.

137

138 Transport characteristics of bacteria were quantified using net speeds $|v_n| = \frac{\sqrt{(x_{t+1}-x_t)^2 + (y_{t+1}-y_t)^2}}{\Delta t}$, turn
 139 angles $\alpha_t = \tan^{-1}\left(\frac{y_{t+2}-y_{t+1}}{x_{t+2}-x_{t+1}}\right) - \tan^{-1}\left(\frac{y_{t+1}-y_t}{x_{t+1}-x_t}\right)$, mean square displacement $MSD(t) = \frac{1}{N}$

140 $\sum_{i=1}^N |r_i(t) - r_i(0)|^2$, velocity autocorrelations $C_v(\tau) = \langle |v_n|(t + \tau) \cdot v(t) \rangle$, average effective dispersion
 141 coefficients $\overline{D^e}(t) = \frac{1}{w\phi} \int_0^w D^e(t, y') dy'$, and bivariate angle-speed probability density contours. Here x_t and
 142 y_t are individual bacteria positions at time t , N is the total number of tracked cells, r_i is the displacement
 143 for bacterium i , and $|v_n|$ is the magnitude of the net velocity (i.e., speed) of the bacteria. D^e reflects the
 144 dispersion coefficient for discrete bins in the y -direction and is used to calculate the average effective
 145 dispersion coefficient by integrating over the width of the domain. The scripts used to calculate all statistics
 146 can be found in Supplementary Methods 2. Note that the net speeds are the speed of the bacteria determined
 147 through particle tracking. Since bacteria are displaced through the porous media both due to their own
 148 motility and the advection imparted by the background flow, the net speed obtained via particle tracking
 149 measures the combined effect of these two drivers.

150 2.2 Micromodel Construction

151 Micromodels for three porous geometries were constructed from PDMS using staggered arrays of grains to
 152 represent porous media (see Fig. 1). The three geometries used in this experiment were **(1)** arrays with a
 153 grain diameter (GD) of 80 μm and a pore throat length (PL) - minimum space between grains - of 20 μm (ϕ
 154 = 0.42), **(2)** arrays with a GD of 40 μm and a PL of 20 μm ($\phi = 0.6$), and **(3)** arrays with a GD of 40 μm
 155 and a PL of 10 μm ($\phi = 0.42$). The micromodel dimensions were 2 mm in the transverse direction, 17 mm
 156 in the longitudinal direction (for the porous section), and 20 μm in the vertical direction. We chose a depth
 157 of 20 μm as we found that a larger depth causes bacteria to move in and out of the focal plane of our camera
 158 too often, and constraining the depth further would have caused excessive shear along the vertical plane.

159 2.3 Bacteria Culture

160 Bacterial strains *Acidovorax* JHL-9 and *Paenibacillus* 300A were grown in liquid culture aerobically at 30
 161 $^\circ\text{C}$ on dextrose-free Trypticase Soy Broth (TSB). At late-log to stationary phase, cultures were diluted to
 162 an optical density at 600 nm (OD600) of $\sim 0.1 - 0.15$ and injected into the micromodel devices described
 163 above. *Geobacter sulfurreducens* was grown anaerobically (80:20 $\text{N}_2:\text{CO}_2$), in glass serum bottles or
 164 headspace vials, crimp-sealed with butyl-rubbers stoppers, on Freshwater Medium⁴³ with 50 mM sodium
 165 fumarate as electron acceptor in place of ferric citrate.⁴⁴ Stationary-phase *G. sulfurreducens* cells were
 166 injected, without dilution, into micromodel devices that had been de-oxygenated overnight in an H_2 -free
 167 anoxic chamber (MBraun, $\text{O}_2 < 10$ ppm, 100% N_2). De-oxygenated micromodels were then removed from
 168 the anoxic chamber using an anaerobic jar and were kept in the anaerobic jar until immediately before use.
 169 *G. sulfurreducens* cells were removed from the serum bottle or headspace vial with a degassed (80:20
 170 $\text{N}_2:\text{CO}_2$) 1-cc syringe and 22-gauge needle and immediately injected into the degassed micromodel.
 171 Though our video acquisition was generally restricted to about an hour after the injection of bacteria, it
 172 should be noted that *G. sulfurreducens* are also known to tolerate and grow with oxygen as a terminal
 173 electron acceptor for up to 24 hours.⁴⁵

174 2.4 Video Acquisition

175 All videos were collected with a confocal imaging technique on a Nikon Eclipse Ti2-U inverted microscope
 176 equipped (viewing vertically downwards and recording motion in the x - y plane) with a digital CMOS
 177 camera Hamamatsu Orca-Flash 4.0 controlled by NIS Elements imaging software. The sensor pixel size
 178 was 6.5 $\mu\text{m} \times 6.5 \mu\text{m}$, and each recorded frame had a size of 2048 pixels \times 2048 pixels. For videos at 10x

179 magnification, the recorded domain size was $2048 \times 6.5/10 = 1331.2 \mu\text{m} \times 1331.2 \mu\text{m}$, and for videos at
180 20x magnification the video domain was $665.6 \mu\text{m} \times 665.6 \mu\text{m}$. Videos were recorded for 5 minutes at
181 frame rates of about 10 frames per second (the interval time between frames varied slightly resulting in
182 rates of 8-12 frames per second). The exact time interval between frames were recorded to allow for
183 accurate computation of transport metrics.

184 **2.5 Image Preprocessing**

185 The raw videos were preprocessed with background subtraction using a lag method specifically developed
186 in-house for these experiments. To capture trajectories of bacteria that may have not moved between two
187 successive frames, the subtracted background must be more than a few frames back in time. Standard
188 practice in background subtraction for such cases is to use the initial frame, or the mean frame, as a
189 background for the rest of the video, but this was not possible in our case due to variability in image
190 brightness throughout the duration of the video. To get around these problems, we used the 5th previous
191 frame to perform background subtraction. In other words, to subtract the background of frame 6, we
192 calculated frame 6 minus frame 1. Thus, any bacteria that moved a little over the course of 5 frames could
193 still be identified in particle tracking.

194 **2.6 Particle Tracking**

195 After background subtraction, the foreground was then loaded into ImageJ and particle tracking was
196 performed with the plugin TrackMate. For feature detection the Laplacian of Gaussian (LoG) detector was
197 used, and to link the features, we used the Linear Assignment Problem (LAP) tracker. A sample output of
198 trajectories from TrackMate is given in the Supplementary Data.

199 **2.7 Flow Field Simulations**

200 Simulations of the flow field were conducted to understand which parts of the geometry bacteria are likely
201 to oversample or undersample. It is important to note that these flow field simulations do not include the
202 motion or presence of bacteria themselves. In other words, we assume that the background flow field is
203 unperturbed by the concentration or kinetics of bacteria. This approach is computationally efficient and
204 provides a baseline for how passive tracers would be advected through the pore space. However, it also
205 means that our simulations neglect the hydrodynamic interactions between bacteria and the fluid or bacteria
206 and the walls. The experimental geometry was initially digitized in Blender then refined in OpenFOAM to
207 produce a regular grid consisting of $2400 \times 2400 \times 72$ voxels with a resolution of $\Delta x = \Delta y = 0.2773 \mu\text{m}$, Δ
208 $z = 0.2778 \mu\text{m}$. The flow fields of the digitized geometries were obtained by solving the flow of
209 incompressible Newtonian fluid governed by the Navier-Stokes equations using SimpleFoam. The steady-
210 state solver belongs to the OpenFOAM package that uses semi-implicit methods for pressure linked
211 equations algorithms. Constant flow rate at specific experimental values of 1 and 5 $\mu\text{L}/\text{h}$ ($Q = 2.78 \times$
212 $10^{-13} \text{m}^3 \text{s}^{-1}$ or $Q = 1.39 \times 10^{-12} \text{m}^3 \text{s}^{-1}$) and constant pressure $P = 0 \text{kg m}^{-1} \text{s}^{-2}$ were imposed at the
213 inlet and outlet of the domain, respectively. No-slip conditions were assigned to the fluid-solid interface.
214 We used a kinematic viscosity ν of $1.14 \times 10^{-6} \text{m}^2/\text{s}$ for the fluid (TSB), given a calculated ratio of $\nu_{\text{TSB}}/$
215 ν_{water} of 1.14.⁴⁶ A sample case folder for the simulations, as well as the commands used to run it on a local
216 machine, can be found in Supplementary Methods 1.

217

218 **3. Results**

219 **3.1 Advection-Dominated Transport Dynamics**

220 We use the term “advection-dominated transport” to highlight a regime wherein the variable shear forces
221 within pore spaces, and dominance of flow speeds over motility speeds, restrict the ability of bacteria to
222 move across streamlines, thus guiding their motion primarily along streamlines at differential velocities.
223 Advection-dominated transport would occur in scenarios of high Peclet number⁴⁷ and persists in situations
224 where weak coupling between motility and biofilm formation patterns are observed.⁴⁸ This type of transport,
225 guided by shear induced cell rotation causing decreased transverse dispersion and increased lateral
226 dispersion, has also been previously reported for bacteria in porous media flows.⁴⁹ Here, we provide
227 additional relevant statistical information to characterize advection-dominated transport for three different
228 species of motile bacteria relevant to bioremediation applications. In the following, we characterize
229 transport dynamics through the (MSD), turn angle distribution, $C_v(\tau)$, and $D^e(t)$. We use these statistics to
230 develop a robust understanding of transport driven by variations in sampled flow speeds, movement of
231 bacteria across streamlines, velocity decorrelation, and spreading.^{50, 51}

232 **3.1.1 Turn Angle Analysis Reveals Impact of Flow Rate on Motility**

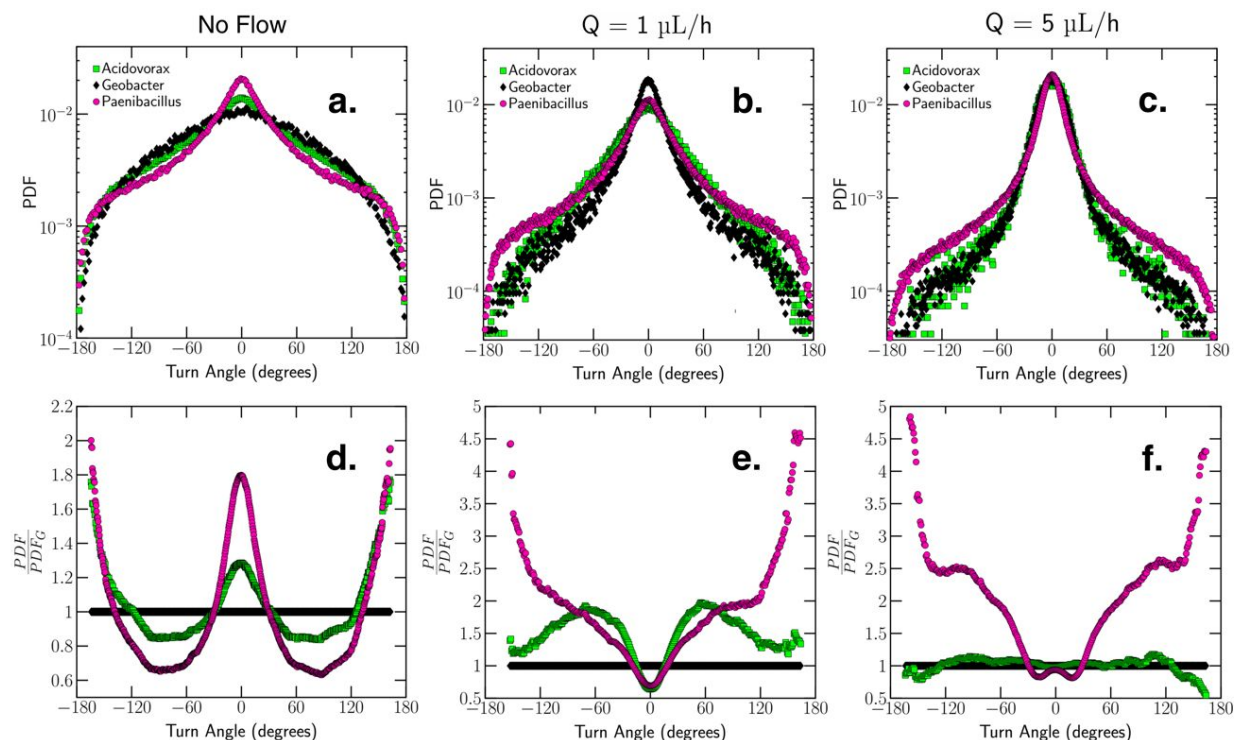
233 To understand the motility of each species of bacteria, we primarily use their turn angle distributions. Note
234 that turn angles as defined in this paper are not the same as traditionally reported turn angles that reflect the
235 body orientation during bacterial run and tumbles.⁵² Because the bacterial speeds are not significantly
236 greater than the background flow speeds, and because our experiments were performed at a relatively low
237 frame rate, we use the term “turn angle” to capture the relative change in the trajectory of advected cells
238 between successive video frames.

239 For no-flow conditions, *Paenibacillus* (peritrichous flagella-based motility) show a high probability of low
240 or very high turn angles ($|\alpha| > 150^\circ$, Fig 2a). In these conditions, low turn angles ($|\alpha| < 30^\circ$) represent
241 persistent forward motion (i.e., long run times), and very high angle turns represent reversals in direction.
242 Although not a necessary condition, a high probability of low turn angles implies a high probability of runs,
243 and a high probability of medium to high turn angles ($|\alpha| > 60^\circ$ and $|\alpha| < 120^\circ$) implies a high probability
244 of random tumbling. *Geobacter* and *Acidovorax* (pili or monotrichous flagella-based motility) have a high
245 probability of medium to high turn angles because their motion is generally more random and is subject to
246 slight changes in hydrodynamics. *Paenibacillus*, on the other hand, show stronger evidence of active
247 exploration strategies in their long runs and complete reversals of direction.

248 To identify the differences in motility for each species more effectively, we also report the ratio of the turn
249 angle PDF for each species to the turn angle PDF for *Geobacter* (Figs. 2d-2f). Essentially, *Geobacter*
250 represents our twitching baseline, as their speed distributions (Supplementary Figure 1) and mean speed
251 (about 2.3 $\mu\text{m/s}$ after subtracting average drift) are generally in agreement with previously reported
252 twitching speeds of various bacteria.^{32, 35-37} Thus, the PDFs of *Acidovorax* and *Paenibacillus* turn angles
253 show departure of their motion behavior from a typical twitcher. When flow is absent (Fig. 2d), the PDF
254 ratio for *Paenibacillus* shows exactly what we expect from a swimmer – high probability of low turn angles
255 (persistent forward motion), low probability of medium turn angles (random motion), and high probability
256 of high turn angles (direction reversal). Intriguingly, the genome of *Acidovorax* JHL-9 (see data
257 availability) contains numerous genes related to twitching motility but not a complement of genes related

258 to flagella-mediated motility. However, as previously discussed, wet mount TEM images of strain JHL-9
 259 (Supplementary Figure 2) suggest the presence of polar flagella. Furthermore, the speed (Supplementary
 260 Figure 1) and turn angle ratio (Fig. 2d) distributions at no-flow indicate that *Acidovorax* behaves differently
 261 than *Geobacter* and closer to *Paenibacillus*, thus revealing distinct motility traits to the three species
 262 selected in this study.

263



264

265 **Figure 2.** Turn angle PDFs for all three species in the low porosity geometry (grain diameter = 80 μm , pore length =
 266 20 μm). (a) Turn angle PDF at flow rate of 0 $\mu\text{L/h}$. (b) Turn angle PDF at flow rate of 1 $\mu\text{L/h}$. (c) Turn angle PDF at
 267 a flow rate of 5 $\mu\text{L/h}$. (d) Turn angle PDF ratio at a flow rate of 0 $\mu\text{L/h}$. (e) Turn angle PDF ratio at a flow rate of 1
 268 $\mu\text{L/h}$. (f) Turn angle PDF ratio at a flow rate of 5 $\mu\text{L/h}$. Turn angle PDF ratios are calculated as the PDF/PDF_G , where
 269 PDF_G represents the PDF of *Geobacter*. We choose to make the ratios relative to *Geobacter* as they move much less
 270 than the other bacteria. Convergence of the shape of the turn angle distribution and clustering of turn angles around
 271 0° at 5 $\mu\text{L/h}$ indicates strong advection-dominated transport.

272

273 Compared to the case of our no-flow experiments, the interpretation of our turn angle distributions in the
 274 presence of flow is slightly more complicated. We posit that in a viscous steady-state flow, non-motile
 275 bacteria would behave as inert particles transported by advection only, thus moving along streamlines of
 276 the pore-scale flow field, which would result in small turn angles between successive steps of the
 277 trajectories. In other words, in presence of a background flow, persistent forward motion means a high
 278 probability of low turn angle distributions. However, motile bacteria also move across streamlines, move
 279 in reverse direction, and explore the pore space under flow conditions, and as a result, large turn angles
 280 should be expected for highly active self-propelled bacteria.^{25, 53-57}

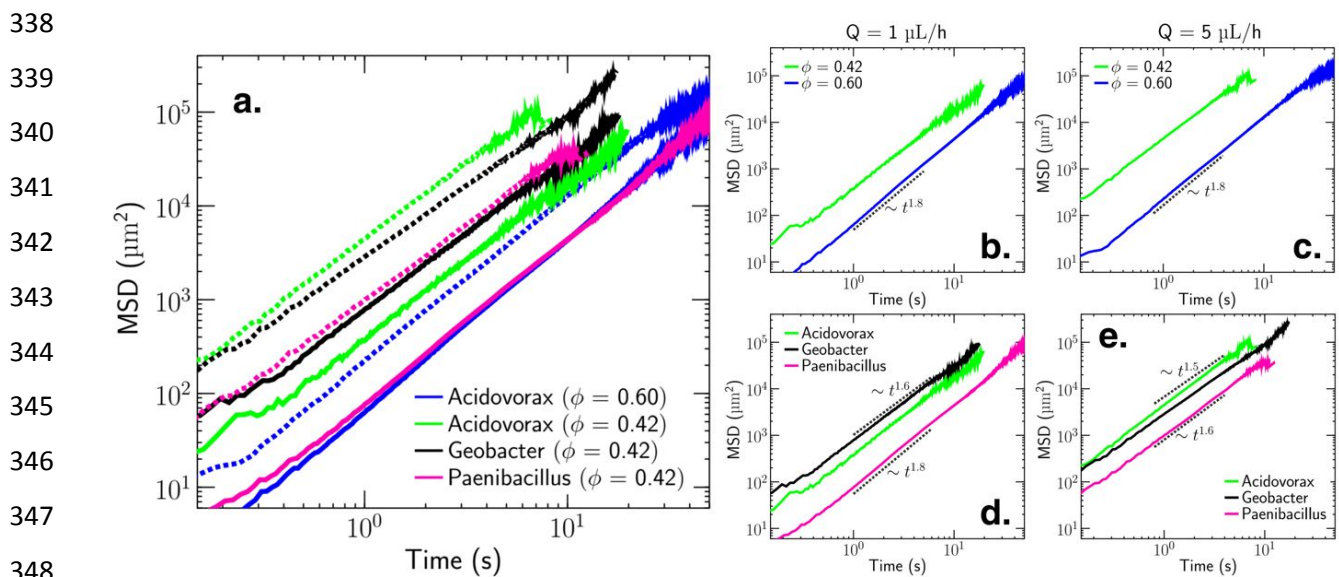
281 We find that *Paenibacillus* have a higher probability of large turns ($\alpha < -90^\circ$ or $\alpha > 90^\circ$) than the other
282 two species at a flow rate of 1 $\mu\text{L/h}$, while at 5 $\mu\text{L/h}$ this difference is even more noticeable (Figs. 2b and
283 2c). Examining the turn angle PDF ratios (Fig. 2e), we see that at 1 $\mu\text{L/h}$ *Paenibacillus* and *Acidovorax* have
284 similar distributions for low to medium turn angles, but *Paenibacillus* has a much higher probability of
285 large turn angles, indicating a greater potential for direction reversal than the other bacteria. At 5 $\mu\text{L/h}$ (Fig.
286 2f) the similarities between *Paenibacillus* and *Acidovorax* completely disappear, and the turn angle PDFs
287 for *Acidovorax* and *Geobacter* essentially converge. This implies that at high flow speeds, *Paenibacillus*,
288 with its peritrichous flagella, are either able to tumble more, or run faster, than *Acidovorax* or *Geobacter*.
289 Furthermore, these results suggest that *Acidovorax*, with its monotrichous flagella, experience a greater
290 impact on its motility due to flow speed than *Paenibacillus* do. While more experiments with a greater
291 variety of monotrichous and peritrichous species are needed to confirm this trend, our initial results imply
292 that peritrichous flagella enable motility at higher flow speeds than monotrichous flagella. Since the no-
293 flow speed PDFs show that *Acidovorax* and *Paenibacillus* have similar max speeds, and monotrichous and
294 amphitrichous bacteria have generally been shown to be capable of higher speeds than peritrichous
295 bacteria,^{36, 58} it does not seem likely that the difference in motility between *Acidovorax* and *Paenibacillus*
296 at high speed is due to run speeds. Thus, our results also imply that at high flow rates *Acidovorax* are unable
297 to tumble, but *Paenibacillus* can. This is supported by research showing that increasing numbers of flagella
298 increases the probability of tumbling.⁵⁹ However, we should also note that differences in the flagellar
299 architecture are not the only possible explanations for differences in the turn angle distributions. Two other
300 possible explanations for this include reorientation strategies, which may impact their preference to run or
301 tumble,⁶⁰ and size-related dynamics, which have been shown to influence hydrodynamic impacts on
302 bacterial motility.⁶¹ As discussed in the introduction, *Geobacter* and *Acidovorax* have similar body lengths,
303 indicating that size is an unlikely reason for the differences observed between these two species. However,
304 the body sizes of *Paenibacillus* are much larger than those of *Geobacter* and *Acidovorax*, indicating that
305 the differences in overall transport observed for *Paenibacillus* may in part be due to their larger body size.
306 Regardless of the exact cause, our results do show that *Paenibacillus* can maintain swimming-like behavior
307 at higher flow rates. *Acidovorax*, on the other hand, act like swimmers at low or no flow, and twitchers at
308 high flow. In other words, advection-dominated transport, which causes trajectories of swimmers to appear
309 similar as trajectories of twitchers, occurs at a lower flow rate for *Acidovorax* than for *Paenibacillus*.

310 3.1.2 Effect on Bacterial Spreading at Different Porosities and Flow Rates

311 Figure 3 confirms additional evidence of advection-dominated transport via the computed MSD. Here, we
312 introduce the term “differential advection” to describe the MSD results, stemming from the bacteria's mixed
313 super-diffusive motions influenced by streamline shifts, trapping, and pore space exploration. This term
314 aptly captures the relationship between velocity decorrelation events and bacterial advection and offers a
315 nuanced understanding of the transport dynamics. As the flow rate increases, bacteria will, on average, have
316 a larger range of displacements due to the magnitudes of velocities it can sample within the laminar profile
317 of porous media flow.¹⁷ Furthermore, smaller turn angles at higher flow rates (as described in the previous
318 section) implies less streamline changing. This results in higher values of the MSD driven by increased
319 differential advection as bacteria are transported by a range of velocities produced by converging and
320 diverging streamlines within the pore network. This term provides a way to highlight the nuances of modes
321 and mechanics of bacterial transport in porous media in addition to examining transport from the lens of
322 Taylor dispersion alone. It also allows us to disentangle the role of lateral dispersion from the roles of

323 bacterial motility, hydrodynamics, and dispersion. Differential advection results in a greater-than-expected
 324 increase in the MSD due to lower likelihood of streamline changing, meaning that bacteria in the fastest
 325 streamlines will advect much more quickly than if they retained their ability to change streamlines. These
 326 observations are further used for later comparisons in the context of Fig. 6, and generally align with
 327 enhanced dispersion reported due to transport of bacteria along faster flow paths than the local flow.^{17, 25}

328 Complementing the increased differential advection, as the flow rate increases, the MSDs of all species of
 329 bacteria in the low porosity geometry show signs of convergence (both in slope and magnitude as seen in
 330 Fig. 3e), likely driven by decorrelation of cell swimming as bacteria navigates pore structures.⁵⁶ Essentially,
 331 advection-dominated transport is thus revealed by the convergence (between different species of bacteria)
 332 of both turn angle distributions and the MSD. In contrast, with the high porosity geometry, we observe less
 333 evidence of MSD convergence, which indicates that the flow speeds are not high enough to suppress
 334 bacterial motility, leading to a reduction in differential advection as shown by lower MSD values (Figs. 3b
 335 and 3c). We also find that for a fixed porosity and flow rate, *Geobacter* and *Acidovorax* always advect more
 336 than *Paenibacillus*, further supporting the idea that peritrichous swimmers are differentially advected to a
 337 lesser degree than twitchers or polar swimmers.



349 **Figure 3.** Mean square displacements (MSDs) at different porosities and flow rates for three different species of
 350 bacteria. **(a)** MSDs from relevant experiments (3 species at lower porosities and 1 at higher porosity, 2 flow rates).
 351 The $1 \mu\text{L/h}$ results are shown as solid lines and the $5 \mu\text{L/h}$ results are shown as dotted lines. b-e split up the plots for
 352 visual comparison purposes. **(b)** MSDs for *Acidovorax* for $\phi = 0.60$ and $\phi = 0.42$ at a flow rate of $1 \mu\text{L/h}$ (mean
 353 fluid speed of $11.6 \mu\text{m/s}$ and $16.5 \mu\text{m/s}$ respectively). **(c)** MSDs for *Acidovorax* for $\phi = 0.60$ and $\phi = 0.42$ at a flow
 354 rate of $5 \mu\text{L/h}$ (mean fluid speeds of $57.9 \mu\text{m/s}$ and $82.7 \mu\text{m/s}$ respectively). **(d)** MSDs for all species for $\phi = 0.42$
 355 at a flow rate of $1 \mu\text{L/h}$. **(e)** MSDs for all species for $\phi = 0.42$ at a flow rate of $5 \mu\text{L/h}$. The rapid increase in MSD driven
 356 by differential advection, along with convergence of the MSDs in the low porosity geometry at $5 \mu\text{L/h}$, provide
 357 evidence of advection-dominated transport. At both flow speeds, *Paenibacillus* show lower values of MSD than
 358 *Geobacter* or *Acidovorax*, indicating a stronger resistance to advection-dominated transport. All low porosity results
 359 in this figure are from the grain diameter = $80 \mu\text{m}$, pore length = $20 \mu\text{m}$ geometry.

360 To further understand spreading in our experiments, we calculated the effective dispersion coefficient, D^e ,
 361 based on the average spatial variance of the bacteria distribution evolving from a point-like injection, that
 362 is, the transport of Green's function as defined in.^{62, 63} At 1 $\mu\text{L/h}$, D^e is impacted by spreading in both the
 363 longitudinal and transverse directions for *Paenibacillus* and *Acidovorax*, but primarily in the longitudinal
 364 direction for *Geobacter* owing to its considerably lower twitching speed than the mean fluid speed. At 5
 365 $\mu\text{L/h}$, D^e primarily represents longitudinal dispersion for all species. Our results show that when the flow
 366 rate increases from 1 $\mu\text{L/h}$ to 5 $\mu\text{L/h}$, D^e increases the most for *Geobacter*, and the least for *Paenibacillus*
 367 (Table 1). Because *Paenibacillus* are able to maintain some form of motility at 5 $\mu\text{L/h}$, and as a result are
 368 still able to change streamlines and explore the pore space, differential advection has less of an impact on
 369 their dispersion than it does for the dispersion of *Geobacter* and *Acidovorax*. In other words, the bacteria
 370 that follow streamlines or explore less space in the transverse direction to the flow, advect and spread more
 371 in the direction of flow. These results complement those presented in,^{17, 25, 49} which showed that
 372 hydrodynamic gradients in porous geometries reduce transverse dispersion. We further this research by
 373 showing that bacterial transport is advective-dominated for a wide variety of flow rates depending on the
 374 type of bacterial motility.

375 **Table 1.** Effective Bacterial Dispersion Coefficients D^e ($\mu\text{m}^2/\text{s}$) for all experiments conducted in the low porosity
 376 geometry ($\phi = 0.42$). As flow rate increases, *Geobacter* have the greatest increase in dispersion and *Paenibacillus*
 377 have the smallest increase in dispersion. As the motility speeds of the bacteria are less than the fluid speed at 5 $\mu\text{L/h}$,
 378 dispersion is almost entirely in the direction of flow for the 5 $\mu\text{L/h}$ experiments.

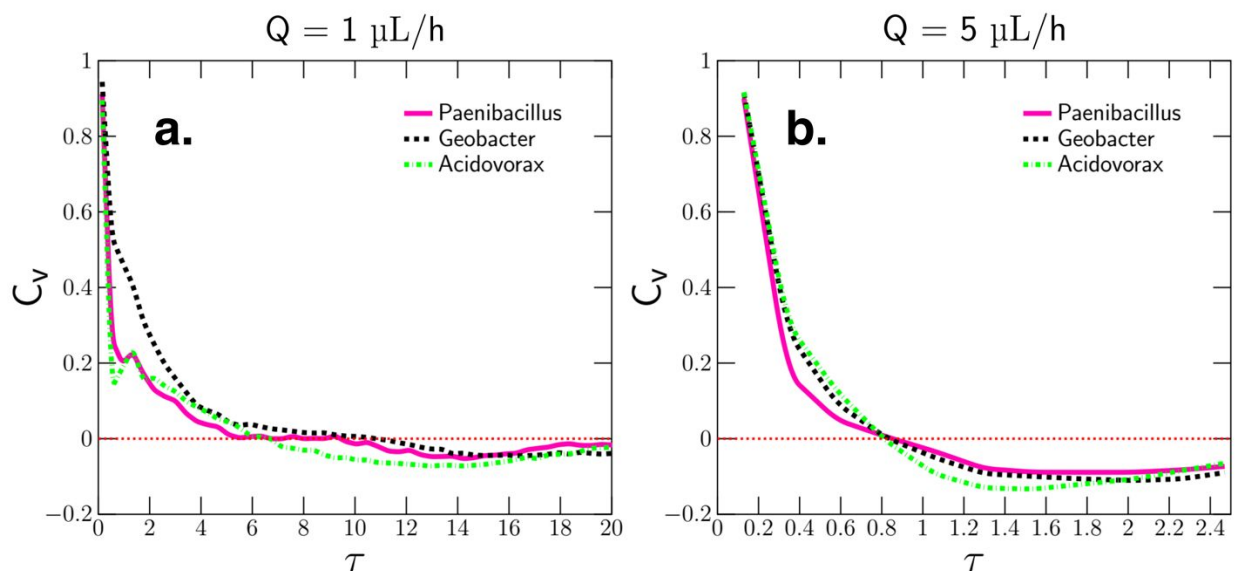
D^e ($\mu\text{m}^2/\text{s}$)	<i>Paenibacillus</i>	<i>Geobacter</i>	<i>Acidovorax</i>
1 $\mu\text{L/h}$	107 \pm 46	308 \pm 97	204 \pm 56
5 $\mu\text{L/h}$	217 \pm 43	895 \pm 148	466 \pm 74

379

380 3.1.3 Velocity Autocorrelation to Examine Emergence of Advection-Dominated Transport

381 We use the velocity autocorrelation function (C_v) to further provide information on advection-dominated
 382 transport.⁶⁴ Generally, in porous media, bacteria show decorrelation in velocities over time due to a
 383 tendency for sampling different portions of the flow field and trapping events (i.e., pore confinement,
 384 occurrence of collisions and attachment to obstacles).^{8, 63} Previous research has shown that decorrelation of
 385 bacterial trajectories is more rapid at high flow rates.⁴⁹ Our findings both confirm these trends and present
 386 new information on how motility type impacts decorrelation. We show that *Paenibacillus* and *Acidovorax*
 387 exhibit decorrelation faster than *Geobacter* at 1 $\mu\text{L/h}$ (Fig. 4a), but that at 5 $\mu\text{L/h}$, all decorrelation times
 388 are essentially the same. This suggests that at low flow rates swimmers experience larger variations in
 389 velocity over time by sampling multiple streamlines and trapping events that decorrelate subsequent
 390 velocities. However, as flow rate increases, motility type no longer has significant impact on decorrelation
 391 events. These observations further support the presence of flagella-based swimming for *Acidovorax* at 1
 392 $\mu\text{L/h}$. Convergence of C_v decorrelation times at high flow rate points to the emergence of advection-
 393 dominated transport. These trends generally agree with the observations of the MSD, D^e and turn angle
 394 distribution analysis, although C_v is slightly less sensitive to differences in motility than the other metrics.

395



396

397 **Figure 4.** Velocity Autocorrelation functions (C_v) for the low porosity experiments at (a) 1 $\mu\text{L}/\text{h}$ and (b) 5 $\mu\text{L}/\text{h}$. At
 398 1 $\mu\text{L}/\text{h}$, the swimming species (*Paenibacillus* and *Acidovorax*) show faster decorrelation time (approximately 6.7
 399 seconds) than the 10.8 second decorrelation time of the twitching species (*Geobacter*). At 5 $\mu\text{L}/\text{h}$ the C_v for the plots
 400 of all species converges producing a decorrelation time of approximately 0.8 seconds, which is further evidence of
 401 advection-dominated transport.

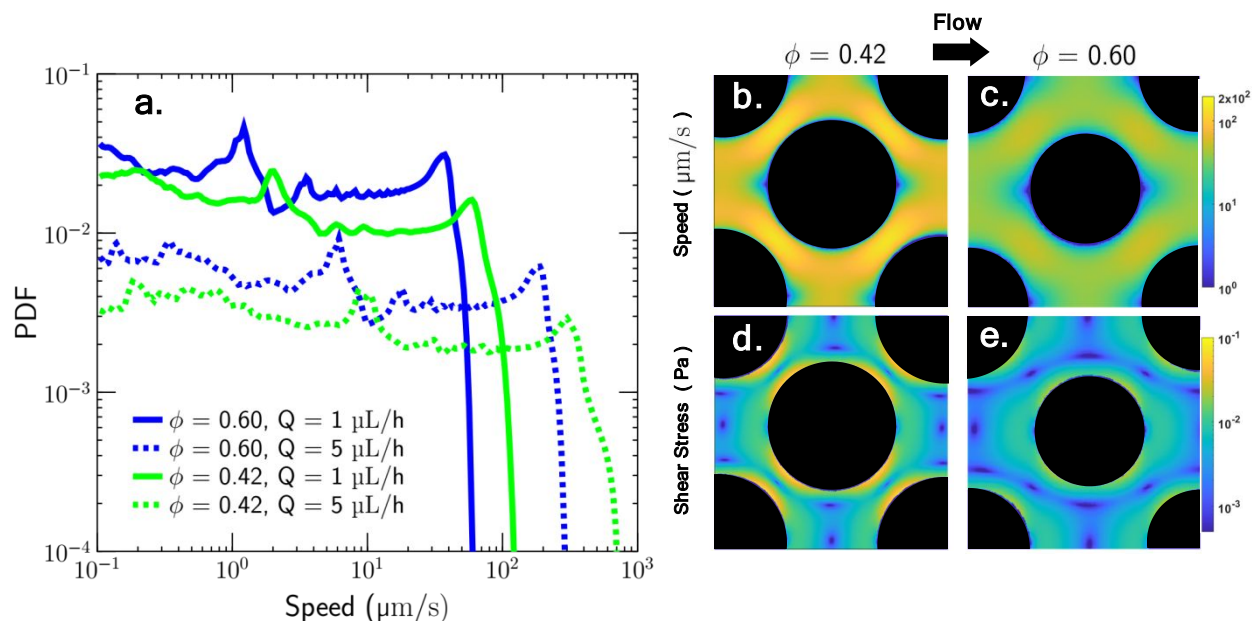
402

403 3.2 Spatial Variations in Net Speeds

404 We digitized the experimental microfluidic geometries and simulated the steady-state viscous flow at high
 405 resolution using SimpleFoam.^{65, 66} to determine how bacteria may under or oversample different parts of a
 406 flow field (Fig. 5). By comparing the obtained simulated distribution of fluid speeds against the
 407 experimentally derived distribution of net bacterial speeds, we can develop an understanding of the zones
 408 within a pore network that bacteria may preferentially occupy. Thus, in this paper we refer to oversampling
 409 as a higher probability in the net bacterial speed PDFs compared to the probability in the simulated flow
 410 speed PDFs at a particular speed. We recognize that a more accurate comparison would use flux weighting
 411 and particle tracking to compare the simulated fluid speed PDFs with the net bacterial speed PDFs.
 412 However, given the large number of trajectories (tens of thousands for each bacteria), and the periodic
 413 nature of our flow field, we posit that the trajectories of tracked bacteria adequately sample the domain
 414 space and thus provide basis for comparison to simulated speeds.

415 We observe that regardless of flow rate, motility type, or porosity, motile bacteria in porous media tend to
 416 undersample low-speed zones and oversample medium-speed zones (relative to the Eulerian fluid speed
 417 PDF) (Fig. 6). This provides additional insight challenging the notion of shear trapping which suggests
 418 bacteria in a shear flow will oversample low-speed zones.^{67, 68} A plausible explanation for this observed
 419 difference lies in recognizing that studies reporting shear trapping were often conducted in simpler
 420 geometries (e.g., straight channels)¹⁴ than in porous media geometries producing converging and diverging

421 streamlines, although it has been reported that shear may lead to creation of hotspot of colonization instead
 422 of trapping close to walls of curved surfaces.¹⁸ However, it is important to note that while our simulations
 423 provide a representation of the flow field structure within the microfluidic geometry, they do not account
 424 for perturbations caused by the bacteria themselves. In reality, motile bacteria generate local disturbances
 425 due to flagellar propulsion, body rotation, and interactions with surfaces. These small-scale effects are
 426 absent from the simulated velocity fields, which may contribute to discrepancies between experimental and
 427 simulated speed distributions in Fig. 6. An exact relationship between hydrodynamics and the observed
 428 speed sampling cannot be deduced in our study because of lack of

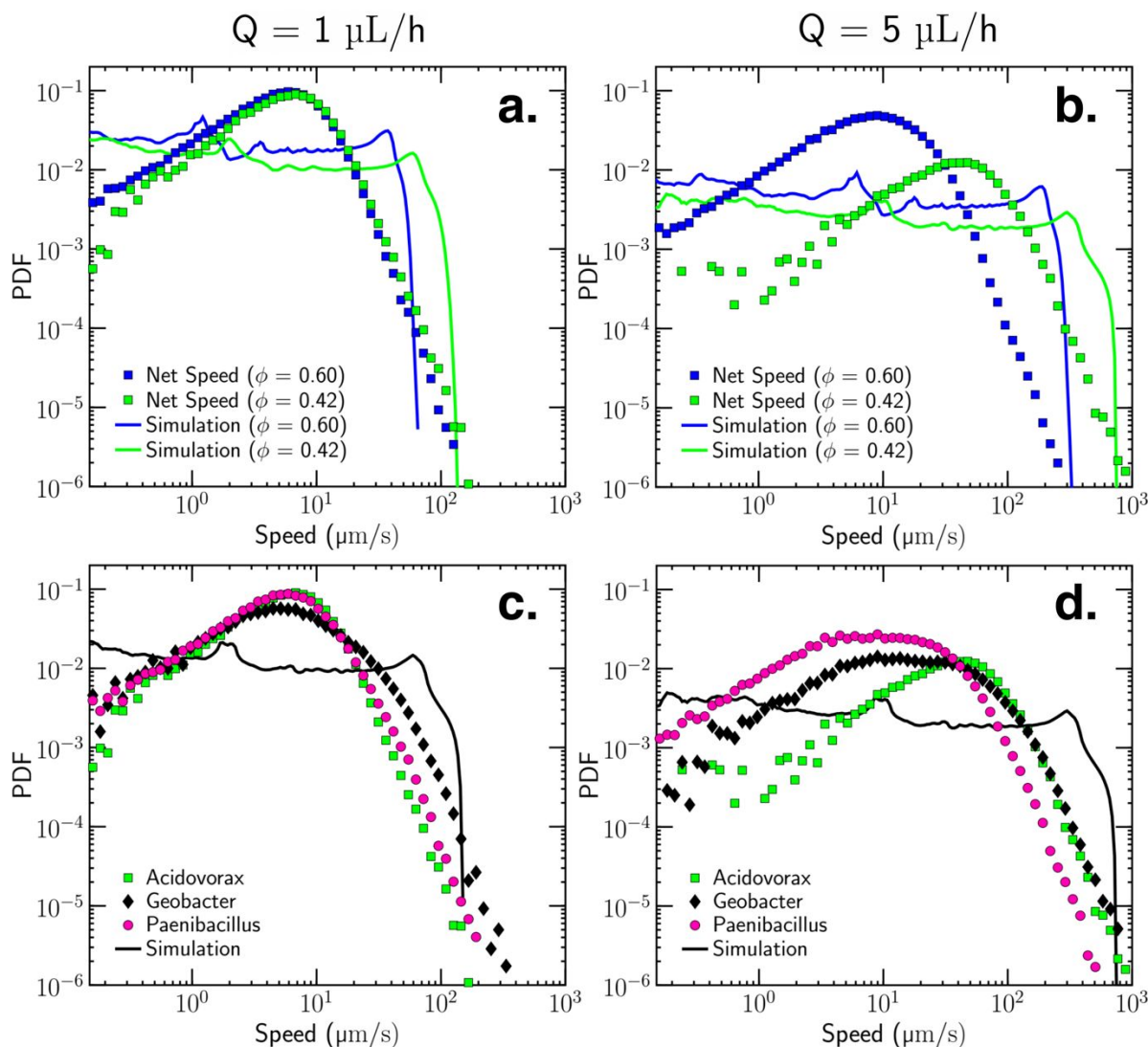


429
 430 **Figure 5.** Results from the steady-state viscous flow simulations of our experimental microfluidic geometries. All low
 431 porosity results in this figure are from the grain diameter = 80 μm , pore length = 20 μm geometry. **(a)** Probability
 432 distribution functions (PDFs) of fluid speed from the simulated flow fields for each porosity and flow rate used in our
 433 experiments. **(b)** Zoomed-in velocity magnitude field for the low porosity simulation at 1 $\mu\text{L}/\text{h}$. **(c)** Zoomed-in velocity
 434 magnitude field for the high porosity simulation at 1 $\mu\text{L}/\text{h}$. **(d)** Zoomed-in shear stress magnitude field for the low
 435 porosity simulation at 1 $\mu\text{L}/\text{h}$. **(e)** Zoomed-in shear stress magnitude field for the high porosity simulation at 1 $\mu\text{L}/\text{h}$.

436
 437 high-resolution tracking necessary to compute shear-induced lateral transport towards the walls due to
 438 Jeffrey orbits⁶⁹⁻⁷¹ and potential backward swimming in the leeward side of the grains, which has been
 439 reported has another form of shear trapping in more complex geometries.¹⁸

440 In no-flow conditions (Supplementary Fig 1), after subtracting drift speeds, *Geobacter* has a mean speed of
 441 2.3 $\mu\text{m}/\text{s}$, *Acidovorax* has a mean speed of 5.9 $\mu\text{m}/\text{s}$, and *Paenibacillus* has a mean speed of 7.2 $\mu\text{m}/\text{s}$. The
 442 95th percentile speed for the three species are 4.5 $\mu\text{m}/\text{s}$, 17.9 $\mu\text{m}/\text{s}$, and 20.6 $\mu\text{m}/\text{s}$ for *Geobacter*,
 443 *Acidovorax*, and *Paenibacillus* respectively. At the low flow rate of 1 $\mu\text{L}/\text{h}$ (16.5 $\mu\text{m}/\text{s}$ average flow speed
 444 at low porosity), the swimming speeds of *Acidovorax* and *Paenibacillus* can thus exceed the fluid flow
 445 speeds (although just barely in the case of *Acidovorax*), but at 5 $\mu\text{L}/\text{h}$, none of the bacteria in our study can
 446 consistently exceed the fluid flow speed. Thus, advection-dominated transport in its simplest form is a result

447 of flow speeds exceeding motility speeds. However, shear adds another layer of complexity when
 448 considering the ability for bacteria to bundle/unbundle their flagella. Recent work has shown that at a shear
 449 magnitude of about 0.26 Pa, *E. Coli* lose control over this mechanism and can't effectively swim.⁷² The 1
 450 $\mu\text{L/h}$ simulations in our study do not produce shear exceeding this value (Figs. 5d and 5e), but at 5 $\mu\text{L/h}$,
 451 the value of shear close to the grain is larger than this threshold value. Although an investigation of
 452 threshold shear magnitudes for bundling abilities in *Paenibacillus* and *Acidovorax* was beyond the scope
 453 of this paper, the inability to control motility⁷³ through bundling/unbundling of flagella remains a likely
 454 explanation for the differences observed in the transport of *Paenibacillus* and *Acidovorax*. Another likely
 455



456
 457 **Figure 6.** PDFs of speeds plotted to show the net speeds of the bacteria overlaid by the simulated speeds for the
 458 respective flow rate and porosity. The net speeds are represented by scatter points, whereas the simulated speeds are
 459 represented by solid lines. All low porosity results in this figure are from the grain diameter = 80 μm , pore length =
 460 20 μm geometry. All simulated PDFs represent the distribution of Eulerian flow speeds for that geometry. (a) Net and

461 simulated speed distributions for *Acidovorax* for $\phi = 0.60$ and $\phi = 0.42$ at a flow rate of 1 $\mu\text{L}/\text{h}$. **(b)** Net and simulated
462 speed distributions for *Acidovorax* for $\phi = 0.60$ and $\phi = 0.42$ and flow rate of 5 $\mu\text{L}/\text{h}$. **(c)** Net and simulated speeds
463 for all species for $\phi = 0.42$ at a flow rate of 1 $\mu\text{L}/\text{h}$. **(d)** Net and simulated speeds for all species for $\phi = 0.42$ at a
464 flow rate of 5 $\mu\text{L}/\text{h}$. These figures show the tendency for motile bacteria to oversample medium-speed zones within a
465 porous media.

466

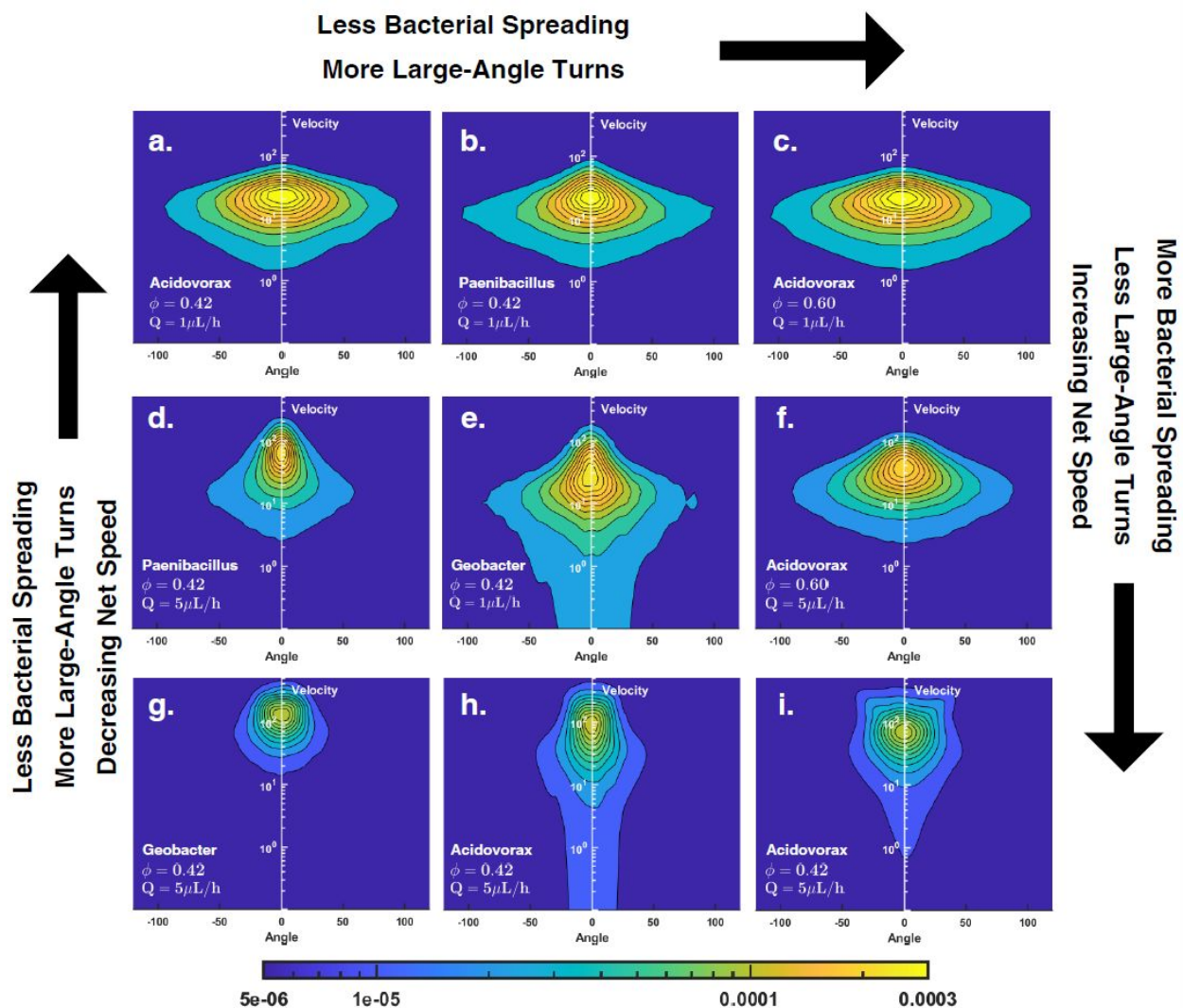
467

468 explanation is that *Paenibacillus* are able to express their motility at higher flow speeds because they can
469 swim faster. However, we show that the 95th percentile of speed distributions for *Acidovorax* (17.9 $\mu\text{m}/\text{s}$)
470 and *Paenibacillus* (20.6 $\mu\text{m}/\text{s}$) are relatively close compared to the mean fluid flow speed in the high flow
471 rate experiment at low porosity (82.7 $\mu\text{m}/\text{s}$), indicating that *Paenibacillus*' ability to express their motility
472 at high flow speeds is more representative of differences in ability to turn (i.e., bundle/unbundle flagella),
473 than because of differences in swimming speed. It should be noted that in our quasi-2D porous media, under
474 uniform and laminar flow, there are no chemotactic or thermal gradients influencing the transport. Thus,
475 the magnitude and distribution of shear within a porous media, which attains its maximum value at grain
476 surfaces and is minimum along centerlines of a pore channel, is likely the primary physical mechanism that
477 controls bacterial transport.

478 **3.3 Combined Effect of Turn Angle and Net Speed on Spreading**

479 We further analyze the combined influence of net speed and turn angle on the advective spreading of motile
480 bacteria using a matrix of bivariate (speed-angle) joint probability density contours (Fig. 7). The probability
481 density matrix allows us to observe general relationships between the differential advection driven
482 spreading plotted in Fig. 3a, and the turn angles and net speeds of the bacteria. As net speed increases,
483 bacteria have a narrower range of turn angles and, therefore, greater spreading in the longitudinal direction
484 stems from strongly advective particle motion. In the top and middle rows of Fig. 7, larger turn angles and
485 less spreading are seen from left to right. In the bottom row, there is no significant change in large-angle
486 turns or advective spreading. Thus, somewhere between the middle and bottom rows, or around a median
487 speed of 50-100 $\mu\text{m}/\text{s}$, the impacts of advection-dominated transport increase to the extent that changes in
488 fluid speed causes insignificant difference in advective spreading or turn angle for bacteria of the same
489 motility type. This suppression in active dispersion in the case of strong fluid flow corroborates recent
490 studies of transport of actively moving particles in porous media.⁷⁴ In addition to providing deeper insight
491 into the transition to the advection-dominated regime, the joint probability density matrix also shows that
492 bacteria are more likely to make large turns at low speeds than at high speeds. Conversely, small-angle
493 turns are more likely to occur at high speeds than large-angle turns. When bacteria are moving with faster
494 streamlines, their turn angles are smaller as they are more likely to go with the flow. When moving with
495 slower streamlines, bacteria are more likely and more able to make large turns and cross transversely to
496 other streamlines. This provides further evidence that pore space exploration and movement across
497 streamlines require low fluid speeds and results in large turn angles.

498



499

500 **Figure 7.** Velocity-angle joint probability density matrix. **(a)** *Acidovorax*, $\phi = 0.42$, $1 \mu\text{L/h}$ (grain diameter = $80 \mu\text{m}$,
 501 pore length = $20 \mu\text{m}$) **(b)** *Paenibacillus*, $\phi = 0.42$, $1 \mu\text{L/h}$ **(c)** *Acidovorax*, $\phi = 0.60$, $1 \mu\text{L/h}$ **(d)** *Paenibacillus*, $\phi =$
 502 0.42 , $5 \mu\text{L/h}$ **(e)** *Geobacter*, $\phi = 0.42$, $1 \mu\text{L/h}$ **(f)** *Acidovorax*, $\phi = 0.60$, $5 \mu\text{L/h}$ **(g)** *Geobacter*, $\phi = 0.42$, $5 \mu\text{L/h}$ **(h)**
 503 *Acidovorax*, $\phi = 0.42$, $5 \mu\text{L/h}$ (grain diameter = $80 \mu\text{m}$, pore length = $20 \mu\text{m}$) **(i)** *Acidovorax*, $\phi = 0.42$, $5 \mu\text{L/h}$ (grain
 504 diameter = $40 \mu\text{m}$, pore length = $10 \mu\text{m}$). Each figure in the density matrix shows probability density contours for net
 505 speed and turn angle for a particular set of conditions. As we move across the matrix from bottom to top, we see
 506 decreased net speeds, increased large-angle turns, and less spreading. As we move from left to right across the matrix,
 507 we see a slight increase in large-angle turns and decrease in spreading, but not as much as going from bottom to top.
 508 There is no significant change in net speed moving from left to right. This figure implies that fast net speeds are
 509 required for bacteria to be in the advection-dominated regime, which results in more small-angle turns. Furthermore,
 510 past a threshold speed of about $50\text{-}100 \mu\text{m/s}$, motile bacteria are unlikely to have large-angle turns.

511

512

513

514 **4. Discussion**

515 This study focuses on investigating the impact of flow rates and porosity on the transport of different species
516 of motile bacteria in porous media. We show that *Geobacter*, with their purely twitching-based motility,
517 understandably need surfaces to propel themselves forward and are unable to swim in suspended media,
518 and as a result are not fast enough in a porous media domain to show any impacts of motility on their
519 transport at low or high flow rates. *Paenibacillus*, with their peritrichous flagella, exhibit strong swimming
520 motility. Although they exhibit weak motion across streamlines and exploration of pore space at high flow
521 rates, their turn angle distributions reflect a higher degree of activity. In the middle of the twitchers and
522 swimmers are *Acidovorax*. Their transport metrics are closer to swimmers at no-flow and at a flow rate of
523 1 $\mu\text{L/h}$, but at 5 $\mu\text{L/h}$, their transport metrics tend to appear closer to twitchers. Although a deep
524 investigation of the motility type of *Acidovorax* is beyond the scope of this work, we show that differences
525 in flagellar architecture offer a reasonable explanation for their behavior. Our results and previous imaging
526 of *Acidovorax* suggest that they have a single polar flagellum as opposed to the peritrichous flagella of
527 *Paenibacillus*. At high flow rates, it appears that peritrichous flagella are more able to facilitate tumbling
528 behavior, and thus, movement across streamlines.

529 In the advection-dominated transport regime, lack of pore space exploration and streamline changing results
530 in less transverse movement and thus leads to an overall increase in transported distance and spread in the
531 direction of flow. We show that advection-dominated transport is revealed through convergence of turn
532 angle distributions, MSDs, species independent velocity decorrelation times, and a clustering of turn angles
533 around 0° . This study also provides contrasting results to the notion of shear trapping wherein motile
534 bacteria are expected to oversample low-velocity regions in a shear flow. In the case of our complex porous
535 geometry, we observe bacteria oversampling medium-speed regions. When the geometry of pore channels
536 allows for convergence and divergence of streamlines in 2D space, producing hydrodynamic patterns
537 typically found in realistic porous media, wide-ranging values of shear forces emerge, leading to an
538 interesting interplay between shear, motility, and the overall bacterial transport. Oversampling of medium-
539 speed zones could be because of high levels of shear (closer to the walls) preventing bacteria from bundling
540 their flagella.⁷² In this unbundled state, the bacteria act as deformable objects resulting in a stokes lift force
541 as they approach surfaces. In addition, size exclusion and hydrodynamic chromatography have shown that
542 the transport of microbes is dependent on size and shape.^{75, 76} Size exclusion occurs because bacteria are
543 too large to only occupy the slow speed zones around the grain.⁷⁷ Unless they are attached, bacteria will
544 move more quickly around the grain than a solute will because part of their body is in higher speed zones.
545 Finally, electrostatic repulsion, or the likely presence of energy barriers close to the grains, may prevent
546 bacteria from getting too close to surfaces.^{18, 55, 78-82} The wide variety of plausible explanations for absence
547 of shear trapping in our study, or shear trapping being manifested through bacterial reorientation in the
548 leeward side of the grains,^{83, 84} illustrate the complexities of analyzing bacterial transport in porous media.
549 The oversampling of medium speeds can thus be a result of several different hydrodynamic or biophysical
550 properties, and we identify shear as a likely physical phenomenon underpinning our observed transport
551 patterns.

552 Our work complements previous studies that have shown advection to dominate the transport of bacteria at
553 high flow rates,^{17, 25} effectively erasing the differences in motile behavior between different species of
554 bacteria.^{14, 18, 67, 78, 85} Our work also builds upon the body of evidence showing that there are significant
555 transport differences between swimmers and twitchers,^{86, 87} and that bacteria with straighter paths (non-

556 motile) spread more (in the direction of flow) than bacteria with exploratory paths (motile) at low flow
557 speeds.^{17, 25} We expect the results presented here to help future researchers in developing more robust
558 experiments and models for not only bioremediation, but other applications where species-aware transport
559 dynamics at small-scale can support and inform development of improved upscaled models. As evidenced
560 by plots of various transport metrics which tend to move towards convergence at high flow rates, it can be
561 argued at sufficiently high flow rates in porous media, different bacterial species will all exhibit uniform
562 transport characteristics not too dissimilar than those expected from passive tracers. The usefulness of the
563 presented research is in recognizing that such high flow rates are rarely encountered in porous media
564 applications, and the progression of bacterial species towards a uniform transport behavior depends on the
565 flow rates, porosities, and the motility types.

566 While we have tried to provide a robust analysis of bacterial transport in idealized porous media under
567 different flow rates, we also recognize that our study contains many limitations. The bacteria were difficult
568 to image and required large exposure times, which resulted in low frame rates and significant light scattering
569 around the grains, thus impacting the accuracy of particle tracking. Furthermore, the low frame rate
570 prevented us from analyzing bacteria through traditional run and tumble statistics. We also recognize that
571 a more expansive set of experiments would have included a wider variety of flow rates (especially lower
572 flow rates so that motility driven diffusion is more dominant than flow driven advection), which would
573 allow for more confidence in any trends observed. Also, although we have mainly attributed the differences
574 in transport of our three species to their differences in motility, there are other phenomena, such as the
575 impact of hydrodynamics on different cell lengths (i.e., size exclusion), and DLVO and steric interactions,⁷
576 which could offer supporting explanations. In addition, we largely neglect the attachment aspect of motility,
577 which may have a large impact on overall transport.^{18, 88} A more rigorous study of the impacts of motility
578 type would use mutant bacteria species only differing in their ability to self-propel, which would allow for
579 a more isolated observation of how motility affects the overall transport. Finally, we recognize that a more
580 complete study of the impacts of flow rate on the transport of different bacteria would examine the impact
581 of shear on the ability for monotrichous and peritrichous flagella to bundle/unbundle. These limitations
582 show that there is still significant work to be done to develop a mature theory of bacterial transport in porous
583 media flows.

584

585 **Data Availability**

586 Besides the raw video and trajectory data, we have provided most of the other data and scripts required to
587 replicate our findings in the supplementary materials. Raw video and trajectory data are available from the
588 corresponding author upon reasonable request. The genome for *Acidovorax* JHL-9 can be found at:
589 https://genome.jgi.doe.gov/portal/AcispJHL9_FD/AcispJHL9_FD.info.html.

590

591 **Conflicts of interest**

592 There are no conflicts of interest to declare.

593

594

595

596 Acknowledgments

597 This research is based upon work supported by the U. S. Department of Energy (DOE) under award number
598 DE-SC0019437. The experiments were performed on a project award
599 (<https://doi.org/10.46936/ltds.proj.2020.51218/60006749>) from the Environmental Molecular Sciences
600 Laboratory (EMSL), a DOE Office of Science User Facility sponsored by the Biological and Environmental
601 Research program, and were partially supported by the Laboratory Directed Research and Development
602 (LDRD) Program at Pacific Northwest National Laboratory. A portion of these data were produced by the
603 US Department of Energy Joint Genome Institute (<https://ror.org/04xm1d337>; operated under Contract No.
604 DE-AC02-05CH11231) in collaboration with the user community. The authors would specifically like to
605 acknowledge the micromodel fabrication help received from Dr. Hardeep Mehta at EMSL and microscopy
606 assistance from EMSL's Tom Wietsma. PNNL is a multi-program national laboratory operated for the U.S.
607 Department of Energy (DOE) by Battelle Memorial Institute under Contract No. DE-AC05-76RL0-1830.
608

609 References

- 610 1. A. Persat, C. D. Nadell, M. K. Kim, F. Ingremeau, A. Siryaporn, K. Drescher, N. S. Wingreen, B.
611 L. Bassler, Z. Gitai, and H. A. Stone. The mechanical world of bacteria. *Cell*, 2015, **161**, 988-997.
- 612 2. P. Yang and J. D. Van Elsas. Mechanisms and ecological implications of the movement of bacteria
613 in soil. *Applied Soil Ecology*, 2018, **129**, 112–120.
- 614 3. S. Jalili-Firoozinezhad, F. S. Gazzaniga, E. L. Calamari, D. M. Camacho, C. W. Fadel, A. Bein, B.
615 Swenor, B. Nestor, M. J. Cronce, A. Tovaglieri, and O. Levy. A complex human gut microbiome
616 cultured in an anaerobic intestine-on-a-chip. *Nat Biomed Eng*, 2019, **3**, 520–531.
- 617 4. J. G. Mitchell and K. Kogure. Bacterial motility: links to the environment and a driving force for
618 microbial physics. *FEMS Microbiology Ecology*, 2006, **55**, 3–16.
- 619 5. T. Jakuszeit and O. A. Croze. Role of tumbling in bacterial scattering at convex obstacles. *Physical*
620 *Review E*, 2024, **109**, 044405.
- 621 6. G. S. Ugolini, M. Wang, E. Secchi, R. Pioli, M. Ackermann, and R. Stocker. Microfluidic
622 approaches in microbial ecology. *Lab on a Chip*, 2024.
- 623 7. V. Tokárová, A. Sudalaiyadum Perumal, M. Nayak, H. Shum, O. Kašpar, K. Rajendran, M.
624 Mohammadi, C. Tremblay, E. A. Gaffney, S. Martel, and D. V. Nicolau Jr. Patterns of bacterial
625 motility in microfluidics-confining environments. *Proc Natl Acad Sci USA*, 2021, **118**,
626 e2013925118.
- 627 8. L. J. Perez, T. Bhattacharjee, S. S. Datta, R. Parashar, and N. L. Sund. Impact of confined
628 geometries on hopping and trapping of motile bacteria in porous media. *Phys Rev E*, 2021, **103**,
629 012611.
- 630 9. T. Bhattacharjee and S. S. Datta. Confinement and activity regulate bacterial motion in porous
631 media. *Soft Matter*, 2019, **15**, 9920-9930.
- 632 10. D. Scheidweiler, F. Miele, H. Peter, T. J. Battin, and P. De Anna. Trait-specific dispersal of bacteria
633 in heterogeneous porous environments: from pore to porous medium scale. *J R Soc Interface*, 2020,
634 **17**, 20200046.

- 635 11. S. Makarchuk, V. C. Braz, N. A. M. Araújo, L. Ciric, and G. Volpe. Enhanced propagation of
636 motile bacteria on surfaces due to forward scattering. *Nat Commun*, 2019, **10**, 4110.
- 637 12. L. J. Perez, R. Parashar, A. Plymale, and T. D. Scheibe. Contributions of biofilm-induced flow
638 heterogeneities to solute retention and anomalous transport features in porous media. *Water*
639 *Research*, 2022, **209**, 117896.
- 640 13. G. Ariel, A. Rabani, S. Benisty, J. D. Partridge, R. M. Harshey, and A. Be'Er. Swarming bacteria
641 migrate by Lévy Walk. *Nat Commun*, 2015, **6**, 8396.
- 642 14. R. Rusconi, J. S. Guasto, and R. Stocker. Bacterial transport suppressed by fluid shear. *Nature*
643 *Phys*, 2014, **10**, 212–217.
- 644 15. M. T. Barry, R. Rusconi, J. S. Guasto, and R. Stocker. Shear-induced orientational dynamics and
645 spatial heterogeneity in suspensions of motile phytoplankton. *J R Soc Interface*, 2015, **12**,
646 20150791.
- 647 16. Y. Yawata, J. Nguyen, R. Stocker, and R. Rusconi. Microfluidic Studies of Biofilm Formation in
648 Dynamic Environments. *J Bacteriol*, 2016, **198**, 2589–2595.
- 649 17. A. Creppy, E. Clément, C. Douarche, M. V. D'Angelo, and H. Auradou. Effect of motility on the
650 transport of bacteria populations through a porous medium. *Phys Rev Fluids*, 2019, **4**, 013102.
- 651 18. E. Secchi, A. Vitale, G. L. Miño, V. Kantsler, L. Eberl, R. Rusconi, and R. Stocker. The effect of
652 flow on swimming bacteria controls the initial colonization of curved surfaces. *Nat Commun*, 2020,
653 **11**, 2851.
- 654 19. R. Rusconi, S. Lecuyer, L. Guglielmini, and H. A. Stone. Laminar flow around corners triggers the
655 formation of biofilm streamers. *J R Soc Interface*, 2010, **7**, 1293–1299.
- 656 20. R. Rusconi, S. Lecuyer, N. Atrusson, L. Guglielmini, and H. A. Stone. Secondary Flow as a
657 Mechanism for the Formation of Biofilm Streamers. *Biophysical Journal*, 2011, **100**, 1392–1399.
- 658 21. D. H. Pieper and W. Reineke. Engineering bacteria for bioremediation. *Current Opinion in*
659 *Biotechnology*, 2000, **11**, 262–270.
- 660 22. T. R. Ginn, B. D. Wood, K. E. Nelson, T. D. Scheibe, E. M. Murphy, and T. P. Clement. Processes
661 in microbial transport in the natural subsurface. *Advances in Water Resources*, 2002, **25**, 1017–
662 1042.
- 663 23. D. Scheidweiler, A. D. Bordoloi, W. Jiao, V. Sentschilo, M. Bollani, A. Chhun, P. Engel, and P. de
664 Anna. Spatial structure, chemotaxis and quorum sensing shape bacterial biomass accumulation in
665 complex porous media. *Nature Communications*, 2024, **15**, 191.
- 666 24. J. Song, Y. Zhang, C. Zhang, X. Du, Z. Guo, Y. Kuang, Y. Wang, P. Wu, K. Zou, L. Zou, and J.
667 Lv. A microfluidic device for studying chemotaxis mechanism of bacterial cancer targeting. *Sci*
668 *Rep*, 2018, **8**, 6394.
- 669 25. M. Dentz, A. Creppy, C. Douarche, E. Clément, and H. Auradou. Dispersion of motile bacteria in
670 a porous medium. *J Fluid Mech*, 2022, **946**, A33.

- 671 26. J. H. Lee, J. K. Fredrickson, A. E. Plymale, A. C. Dohnalkova, C. T. Resch, J. P. McKinley, and
672 L. Shi. An autotrophic H₂-oxidizing, nitrate-respiring, Tc(VII)-reducing *Acidovorax* sp. isolated
673 from a subsurface oxic-anoxic transition zone. *Environmental Microbiology Reports*, 2015, **7**, 395–
674 403.
- 675 27. F. Caccavo Jr, D. J. Lonergan, D. R. Lovley, M. Davis, J. F. Stolz, and M. J. McInerney. *Geobacter*
676 *sulfurreducens* sp. nov., a hydrogen- and acetate-oxidizing dissimilatory metal-reducing
677 microorganism. *Appl Environ Microbiol*, 1994, **60**, 3752–3759.
- 678 28. B. Ahmed, B. Cao, J. S. McLean, T. Ica, A. Dohnalkova, O. Istanbulu, A. Paksoy, J. K.
679 Fredrickson, and H. Beyenal. Fe(III) Reduction and U(VI) Immobilization by *Paenibacillus* sp.
680 Strain 300A, Isolated from Hanford 300A Subsurface Sediments. *Appl Environ Microbiol*, 2012,
681 **78**, 8001–8009.
- 682 29. E. Krawczyk-Bärsch, U. Gerber, K. Müller, H. Moll, A. Rossberg, R. Steudtner, and M. L.
683 Merroun. Multidisciplinary characterization of U(VI) sequestration by *Acidovorax facilis* for
684 bioremediation purposes. *Journal of Hazardous Materials*, 2018, **347**, 233–241.
- 685 30. B. A. Methe, K. E. Nelson, J. A. Eisen, I. T. Paulsen, W. Nelson, J. F. Heidelberg, D. Wu, M. Wu,
686 N. Ward, M. J. Beanan, R. J. Dodson, R. Madupu, L. M. Brinkac, S. C. Daugherty, R. T. DeBoy,
687 A. S. Durkin, M. Gwinn, J. F. Kolonay, S. A. Sullivan, D. H. Haft, J. Selengut, T. M. Davidsen, N.
688 Zafar, O. White, B. Tran, C. Romero, H. A. Forberger, J. Weidman, H. Khouri, T. V. Feldblyum,
689 T. R. Utterback, S. E. Van Aken, D. R. Lovley, and C. M. Fraser. Genome of *Geobacter*
690 *sulfurreducens*: Metal Reduction in Subsurface Environments. *Science*, 2003, **302**, 1967–1969.
- 691 31. M. Govarthanan, R. Mythili, T. Selvankumar, S. Kamala-Kannan, A. Rajasekar, and Y. C. Chang.
692 Bioremediation of heavy metals using an endophytic bacterium *Paenibacillus* sp. RM isolated from
693 the roots of *Tridax procumbens*. *3 Biotech*, 2016, **6**, 242.
- 694 32. F. Jin, J. C. Conrad, M. L. Gibiansky, and G. C. Wong. Bacteria use type-IV pili to slingshot on
695 surfaces. *Proceedings of the National Academy of Sciences*, 2011, **108**, 12617-12622.
- 696 33. A. M. Speers, B. D. Schindler, J. Hwang, A. Genc, and G. Reguera. Genetic identification of a PilT
697 motor in *Geobacter sulfurreducens* reveals a role for pilus retraction in extracellular electron
698 transfer. *Frontiers in microbiology*, 2016, **7**, 1578.
- 699 34. E. N. Grady, J. MacDonald, L. Liu, A. Richman, and Z. C. Yuan. Current knowledge and
700 perspectives of *Paenibacillus*: a review. *Microbial cell factories*, 2016, **15**, 1-18.
- 701 35. P. G. Jayathilake, B. Li, P. Zuliani, T. Curtis, and J. Chen. Modelling bacterial twitching in fluid
702 flows: a CFD-DEM approach. *Scientific reports*, 2019, **9**, 14540.
- 703 36. S. Nakamura. Spirochete flagella and motility. *Biomolecules*, 2020, **10**, 550.
- 704 37. O. Bahar, L. De La Fuente, and S. Burdman. Assessing adhesion, biofilm formation and motility
705 of *Acidovorax citrulli* using microfluidic flow chambers. *FEMS Microbiology letters*, 2010, **312**,
706 33-39.

- 707 38. S. Wang, P. R. Jaffe, G. Li, S. W. Wang, and H. A. Rabitz. Simulating bioremediation of uranium-
708 contaminated aquifers; uncertainty assessment of model parameters. *Journal of Contaminant*
709 *Hydrology*, 2003, **64**, 283-307.
- 710 39. S. B. Yabusaki, Y. Fang, K. H. Williams, C. J. Murray, A. L. Ward, R. D. Dayvault, S. R. Waichler,
711 D. R. Newcomer, F. A. Spane, and P. E. Long. Variably saturated flow and multicomponent
712 biogeochemical reactive transport modeling of a uranium bioremediation field experiment. *Journal*
713 *of contaminant hydrology*, 2011, **126**, 271-290.
- 714 40. Y. Liu, M. Du, S. Shu, J. Wei, K. Zhu, and G. Wang. Bacterial surface properties and transport
715 behavior actively respond to an extracellular polymeric substance gradient in saturated porous
716 media. *Science of The Total Environment*, 2024, 173889.
- 717 41. X. Yang, R. Parashar, N. L. Sund, A. E. Plymale, T. D. Scheibe, D. Hu, and R. T. Kelly. On
718 Modeling Ensemble Transport of Metal Reducing Motile Bacteria. *Sci Rep*, 2019, **9**, 14638.
- 719 42. J. Y. Tinevez, N. Perry, J. Schindelin, G. M. Hoopes, G. D. Reynolds, E. Laplantine, S. Y.
720 Bednarek, S. L. Shorte, and K. W. Eliceiri. TrackMate: An open and extensible platform for single-
721 particle tracking. *Methods*, 2017, **115**, 80–90.
- 722 43. D. R. Lovley and E. J. P. Phillips. Novel mode of microbial energy metabolism: organic carbon
723 oxidation coupled to dissimilatory reduction of iron or manganese. *Appl Environ Microbiol*, 1988,
724 **54**, 1472-1480.
- 725 44. A. E. Plymale, V. L. Bailey, J. K. Fredrickson, S. M. Heald, E. C. Buck, L. Shi, Z. Wang, C. T.
726 Resch, D. A. Moore, and H. Bolton Jr. Biotic and Abiotic Reduction and Solubilization of
727 Pu(IV)O₂•xH₂O(am) as Affected by Anthraquinone-2,6-disulfonate (AQDS) and
728 Ethylenediaminetetraacetate (EDTA). *Environ Sci Technol*, 2012, **46**, 2132–2140.
- 729 45. W. C. Lin, M. V. Coppi, and D. R. Lovley. *Geobacter sulfurreducens* Can Grow with Oxygen as a
730 Terminal Electron Acceptor. *Appl Environ Microbiol*, 2004, **70**, 2525-2528.
- 731 46. M. M. Thornton, H. M. Chung-Esaki, C. B. Irvin, D. M. Bortz, M. J. Solomon, and J. G. Younger.
732 Multicellularity and antibiotic resistance in *Klebsiella pneumoniae* grown under bloodstream-
733 mimicking fluid dynamic conditions. *The Journal of infectious diseases*, 2012, **206**, 588-595.
- 734 47. I. Tuval, L. Cisneros, C. Dombrowski, C. W. Wolgemuth, J. O. Kessler, and R. E. Goldstein.
735 Bacterial swimming and oxygen transport near contact lines. *Proceedings of the National Academy*
736 *of Sciences*, 2005, **102**, 2277-2282.
- 737 48. T. Rossy, C. D. Nadell, and A. Persat. Cellular advective-diffusion drives the emergence of
738 bacterial surface colonization patterns and heterogeneity. *Nature communications*, 2019, **10**, 2471.
- 739 49. A. Dehkharghani, N. Waisbord, J. Dunkel, and J. S. Guasto. Bacterial scattering in microfluidic
740 crystal flows reveals giant active Taylor–Aris dispersion. *Proceedings of the National Academy of*
741 *Sciences*, 2019, **116**, 11119-11124.
- 742 50. A. Einstein. On the Movement of Small Particles Suspended in Stationary Liquids Required by the
743 Molecular-Kinetic Theory of Heat. *Annalen Der Physik*, 1905, 549–560.

- 744 51. K. J. Duffy and R. M. Ford. Turn angle and run time distributions characterize swimming behavior
745 for *Pseudomonas putida*. *J Bacteriol*, 1997, **179**, 1428–1430.
- 746 52. H. C. Berg and D. A. Brown. Chemotaxis in *Escherichia coli* analysed by three-dimensional
747 tracking. *Nature*, 1972, **239**, 500–504.
- 748 53. M. W. Becker, D. W. Metge, S. A. Collins, A. M. Shapiro, and R. W. Harvey. Bacterial Transport
749 Experiments in Fractured Crystalline Bedrock. *Ground Water*, 2003, **41**, 682–689.
- 750 54. J. Liu, R. M. Ford, and J. A. Smith. Idling Time of Motile Bacteria Contributes to Retardation and
751 Dispersion in Sand Porous Medium. *Environ Sci Technol*, 2011, **45**, 3945–3951.
- 752 55. J. C. Conrad and R. Poling-Skutvik. Confined Flow: Consequences and Implications for Bacteria
753 and Biofilms. *Annu Rev Chem Biomol Eng*, 2018, **9**, 175–200.
- 754 56. A. Dehkharghani, N. Waisbord, and J. S. Guasto. Self-transport of swimming bacteria is impaired
755 by porous microstructure. *Commun Phys*, 2023, **6**, 18.
- 756 57. R. M. Ford and R. W. Harvey. Role of chemotaxis in the transport of bacteria through saturated
757 porous media. *Advances in Water Resources*, 2008, **30**, 1608–1617.
- 758 58. K. Bente, S. Mohammadinejad, M. A. Charsooghi, F. Bachmann, A. Codutti, C. T. Lefèvre, S.
759 Klumpp, and D. Faivre. High-speed motility originates from cooperatively pushing and pulling
760 flagella bundles in bilophotrichous bacteria. *Elife*, 2020, **9**, e47551.
- 761 59. J. Najafi, M. R. Shaebani, T. John, F. Altegoer, G. Bange, and C. Wagner. Flagellar number governs
762 bacterial spreading and transport efficiency. *Sci Adv*, 2018, **4**, eaar6425.
- 763 60. J. G. Mitchell. The energetics and scaling of search strategies in bacteria. *The American Naturalist*,
764 2002, **160**, 727–740.
- 765 61. T. Kaya and H. Koser. Direct upstream motility in *Escherichia coli*. *Biophysical journal*, 2012, **102**,
766 1514–1523.
- 767 62. L. J. Perez, J. J. Hidalgo, and M. Dentz. Upscaling of mixing-limited bimolecular chemical
768 reactions in Poiseuille flow. *Water Resources Research*, 2019, **55**, 249–269.
- 769 63. A. Puyguiraud, L. J. Perez, J. J. Hidalgo, and M. Dentz. Effective dispersion coefficients for the
770 upscaling of pore-scale mixing and reaction. *Advances in Water Resources*, 2020, **146**, 103782.
- 771 64. S. C. Weber, M. A. Thompson, W. E. Moerner, A. J. Spakowitz, and J. A. Theriot. Analytical tools
772 to distinguish the effects of localization error, confinement, and medium elasticity on the velocity
773 autocorrelation function. *Biophysical journal*, 2012, **102**, 2443–2450.
- 774 65. H. G. Weller, G. Tabor, H. Jasak, and C. Fureby. A tensorial approach to computational continuum
775 mechanics using object-oriented techniques. *Comput Phys*, 1998, **12**, 620.
- 776 66. OpenFOAM Foundation. OpenFOAM: Open-source CFD software, <https://openfoam.org/>,
777 (accessed 2023).
- 778 67. L. Vennamneni, S. Nambiar, and G. Subramanian. Shear-induced migration of microswimmers in
779 pressure-driven channel flow. *Journal of Fluid Mechanics*, 2020, **890**, A15.

- 780 68. M. Lee, C. Lohrmann, K. Szuttor, H. Auradou, and C. Holm. The influence of motility on bacterial
781 accumulation in a microporous channel. *Soft Matter*, 2021, **17**, 893-902.
- 782 69. G. B. Jeffery. The motion of ellipsoidal particles immersed in a viscous fluid. *Proceedings of the*
783 *Royal Society of London. Series A*, 1922, **102**, 161-179.
- 784 70. T. J. Pedley and J. O. Kessler. Hydrodynamic phenomena in suspensions of swimming
785 microorganisms. *Annual Review of Fluid Mechanics*, 1992, **24**, 313-358.
- 786 71. A. Choudhary, S. Paul, F. Rühle, and H. Stark. How inertial lift affects the dynamics of a
787 microswimmer in Poiseuille flow. *Communications Physics*, 2022, **5**, 14.
- 788 72. J. Yang, K. Kikuchi, and T. Ishikawa. High shear flow prevents bundling of bacterial flagella and
789 induces lateral migration away from a wall. *Communications Physics*, 2023, **6**, 354.
- 790 73. N. A. Licata, B. Mohari, C. Fuqua, and S. Setayeshgar. Diffusion of bacterial cells in porous media.
791 *Biophysical journal*, 2016, **110**, 247-257.
- 792 74. R. Alonso-Matilla, B. Chakrabarti, and D. Saintillan. Transport and dispersion of active particles
793 in periodic porous media. *Physical Review Fluids*, 2019, **4**, 043101.
- 794 75. T. H. Weiss, A. L. Mills, G. M. Hornberger, and J. S. Herman. Effect of bacterial cell shape on
795 transport of bacteria in porous media. *Environmental science & technology*, 1995, **29**, 1737-1740.
- 796 76. D. E. Fontes, A. L. Mills, G. M. Hornberger, and J. S. Herman. Physical and chemical factors
797 influencing transport of microorganisms through porous media. *Applied and Environmental*
798 *Microbiology*, 1991, **57**, 2473-2481.
- 799 77. F. Grant Ferris, N. Szponar, and B. A. Edwards. *Groundwater Microbiology*. The Groundwater
800 Project, 2021.
- 801 78. M. Molaei and J. Sheng. Succeed escape: Flow shear promotes tumbling of Escherichia coli near a
802 solid surface. *Sci Rep*, 2016, **6**, 35290.
- 803 79. W. P. Johnson, K. A. Blue, B. E. Logan, and R. G. Arnold. Modeling Bacterial Detachment During
804 Transport Through Porous Media as a Residence-Time-Dependent Process. *Water Resour Res*,
805 1995, **31**, 2649–2658.
- 806 80. H. Dong, T. D. Scheibe, W. P. Johnson, C. M. Monkman, and M. E. Fuller. Change of Collision
807 Efficiency with Distance in Bacterial Transport Experiments. *Ground Water*, 2006, **44**, 415–429.
- 808 81. M. Hermansson. The DLVO theory in microbial adhesion. *Colloids and Surfaces B: Biointerfaces*,
809 1999, **14**, 105–119.
- 810 82. A. Zöttl and H. Stark. Nonlinear dynamics of a microswimmer in Poiseuille flow. *Physical review*
811 *letters*, 2012, **108**, 218104.
- 812 83. M. Lee, C. Lohrmann, K. Szuttor, H. Auradou, and C. Holm. The influence of motility on bacterial
813 accumulation in a microporous channel. *Soft Matter*, 2021, **17**, 893-902.
- 814 84. G. L. Miño, M. D. Baabour, R. H. Chertcoff, G. O. Gutkind, E. Clément, H. Auradou, and I. P.
815 Ippolito. E. coli accumulation behind an obstacle. 2018.

- 816 85. P. de Anna, A. A. Pahlavan, Y. Yawata, R. Stocker, and R. Juanes. Chemotaxis under flow disorder
817 shapes microbial dispersion in porous media. *Nat Phys*, 2021, **17**, 68–73.
- 818 86. K. Son, D. R. Brumley, and R. Stocker. Live from under the lens: exploring microbial motility with
819 dynamic imaging and microfluidics. *Nature Reviews Microbiology*, 2015, **13**, 761–775.
- 820 87. N. Lu, T. Bevard, A. Massoudieh, C. Zhang, A. C. Dohnalkova, J. L. Zilles, and T. H. Nguyen.
821 Flagella-Mediated Differences in Deposition Dynamics for *Azotobacter vinelandii* in porous
822 media. *Environ Sci Technol*, 2013, **47**, 5162–5170.
- 823 88. A. N. Simsek, M. D. Koch, J. E. Sanfilippo, Z. Gitai, G. Gompper, and B. Sabass. Bacteria tune a
824 trade-off between adhesion and migration to colonize surfaces under flow. *PRX Life*, 2024, **2**,
825 023003.

Data Availability

Besides the raw video and trajectory data, we have provided most of the other data and scripts required to replicate our findings in the supplementary materials. Raw video and trajectory data are available from the corresponding author upon reasonable request. The genome for *Acidovorax* JHL-9 can be found at: https://genome.jgi.doe.gov/portal/AcispJHL9_FD/AcispJHL9_FD.info.html.